THE JOURNAL OF PHYSICAL CHEMISTRY B

Article

pubs.acs.org/JPCB

Structural Heterogeneity and Unique Distorted Hydrogen Bonding in Primary Ammonium Nitrate Ionic Liquids Studied by High-Energy X-ray Diffraction Experiments and MD Simulations

Xuedan Song,[†] Hiroshi Hamano,[†] Babak Minofar,[†] Ryo Kanzaki,[‡] Kenta Fujii,[§] Yasuo Kameda,[∥] Shinji Kohara,[⊥] Masayoshi Watanabe,[#] Shin-ichi Ishiguro,[†] and Yasuhiro Umebayashi*,[†]

[†]Department of Chemistry, Faculty of Science, Kyushu University, Hakozaki, Higashi-ku, Fukuoka 812-8581, Japan

[‡]Graduate School of Science and Engineering, Kagoshima University, Korimoto, Kagoshima 890-0065, Japan

[§]Neutron Science Laboratory, Institute for Solid State Physics, The University of Tokyo, Kashiwanoha, Kashiwa-shi, Chiba 277-8581, Japan

[∥]Department of Material and Biological Chemistry, Faculty of Science, Yamagata University, Kojirakawa-machi 1-4-12, Yamagata 990-8560, Japan

[⊥]Japan Synchrotron Radiation Research Institute (JASRI), Sayo-cho, Sayo-gun, Hyogo 679-5198, Japan

[#]Department of Chemistry and Biotechnology, Yokohama National University, 79-5 Tokiwadai Hodogaya-ku, Yokohama 240-8501, Japan

Supporting Information

ABSTRACT: Liquid structure and the closest ion−ion interactions in a series of primary alkylammonium nitrate ionic liquids $[C_nAm^+][NO_3^-]$ (n = 2, 3, and 4) were studied by means of high-energy X-ray diffraction (HEXRD) experiments with the aid of molecular dynamics (MD) simulations. Experimental density and X-ray structure factors are in good accordance with those evaluated with MD simulations. With regard to liquid structure, characteristic peaks appeared in the low Q (Q: a scattering vector) region of X-ray structure factors $S(Q)$'s for all ionic liquids studied here, and they increased in intensity with a peak position shift toward the lower Q side by increasing the alkyl chain length. Experimentally evaluated $S^{Q_{peak}}(r_{max})$ functions, which represent the $S(Q)$ intensity at a peak position of maximum intensity Q_{peak} as a function of distance (actually a integration range r_{max}), revealed that characteristic peaks in the low Q region are related to the intermolecular anion−anion correlation decrease in the r range of 10−12 Å. Appearance of the peak in the low Q region is probably related to the exclusion of the correlations among ions of the same sign in this r range by the alkyl chain aggregation. From MD simulations, we found unique and rather distorted NH···O hydrogen bonding between C_nAm^+ (n = 2, 3, and 4) and NO_3^- in these ionic liquids regardless of the alkyl chain length. Subsequent ab initio calculations for both a molecular complex $C_2H_5NH_2\cdots HONO_2$ and an ion pair $C_2H_5NH_3^+\cdots ONO_2^-$ revealed that such distorted hydrogen bonding is specific in a liquid state of this family of ionic liquids, though the linear orientation is preferred for both the N···HO hydrogen bonding in a molecular complex and the NH···O one in an ion pair. Finally, we propose our interpretation of structural heterogeneity in PILs and also in APILs.

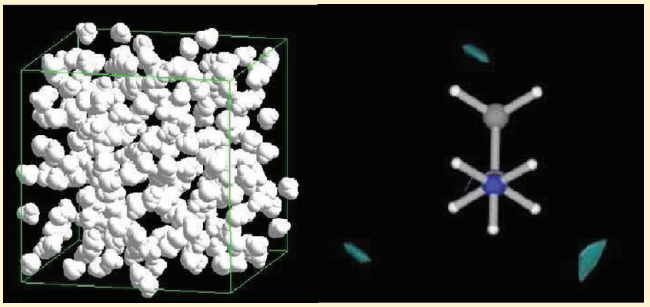

INTRODUCTION

Room-temperature ionic liquids (RTILs) have been receiving much attention as new functionalized solvents in various fields due to their unique properties.[1−4] In terms of dissociable hydrogen atoms, RTILs can be classified into two categories like nonaqueous molecular solvents, i.e., aprotic (APILs) and protic (PILs) ones, respectively. PILs can be simply prepared by mixing a Brønsted acid HA and a Brønsted base B to yield onium salts $[HB^+][A^-]$ by proton transfer.[5−7] They have attracted attention as new proton conductive materials for fuel cells[8,9] and catalytic solvents for organic syntheses.[10] Many reviews about PILs have been published.[11−13]

One of the most well-known PILs is ethylammonium nitrate ($[C_2Am^+][NO_3^-]$), which was reported in 1914 for the first time by Walden et al.[14] $[C_2Am^+][NO_3^-]$ has been used as the solvent free electrolyte for a fuel cell.[15] Other applications have been also reported such as media for amphiphile self-assembly,[16,17] catalysts for organic reactions,[18] and solvents for enzyme reactions.[19] Macroscopic physicochemical properties of $[C_2Am^+][NO_3^-]$ have been predicted with ab initio

Received: October 4, 2011
Revised: February 9, 2012
Published: February 29, 2012

dx.doi.org/10.1021/jp209561t | J. Phys. Chem. B 2012, 116, 2801−2813

calculations,[20] and transport and thermodynamic properties were experimentally investigated such as viscosity,[15,21−23] ionic conductivity,[15,22,23] melting point,[22,23] liquid surface tension,[16,22] and refractive index.[21,22] Various solvent parameters[21,24] and the Hammett acidity function[25−27] have been evaluated. ΔpK_a, which is defined as the difference of acid dissociation constants for HB^+ and HA in the respective aqueous solution, is currently proposed as one of the measures for the ion−ion interaction and the Brønsted acid−base property of PILs.[23,28,29] We have reported the thermodynamics of autoprotolysis reaction in $[C_2Am^+][NO_3^-]$; $C_2H_5NH_3^+ + NO_3^- \leftrightharpoons C_2H_5NH_2 + HNO_3$.[30−32] Although the reaction enthalpy ΔH° for the autoprotolysis in $[C_2Am^+][NO_3^-]$ is more positive than that in water, the corresponding Gibbs free energy ΔG° is significantly more negative than that in water. This behavior is due to the difference in reaction entropy (positive reaction entropy in $[C_2Am^+][NO_3^-]$, whereas negative in water). Thus, the thermodynamics of autoprotolysis in $[C_2Am^+][NO_3^-]$ suggests desolvation of the component ions from the produced neutral products $C_2H_5NH_2$ and HNO_3 yields larger entropy to make the reaction favorable relative to that in water. We have also studied the liquid structure of $[C_2Am^+][NO_3^-]$ by large angle X-ray scattering (LAXS) experiments and molecular dynamics (MD) simulations.[33]

On the structural viewpoint, Ludwig et al. have measured far-IR spectra of $[C_nAm^+][NO_3^-]$ (n = 2 and 3) and ascribed broad bands observed in the far-IR range to the intermolecular vibrations.[34,35] Atkin et al. have reported small-angle neutron scattering (SANS) experiments on ammonium deuterated $[C_nAm^+][NO_3^-]$ (n = 2 and 3), and found that the specific peaks at Q = 0.66 and 0.54 $Å^{-1}$ appeared in SANS profiles for n = 2 and 3, respectively.[36] On the basis of this observation, they proposed that these ionic liquids act as the "*smallest amphiphiles*"; i.e., the ethyl and the propyl groups in the cations aggregate to form nonpolar domains in these neat ionic liquids, while polar domains consist of an ammonium moiety of the cation and the nitrate anion. In fact, our LAXS experiments and MD simulations suggest that the ethyl groups in neat $[C_2Am^+][NO_3^-]$ are significantly correlated.[33] Greaves et al. recorded small- and wide-angle X-ray scattering (SWAXS) of 20 different PILs, and found that most of the PILs have a nanoscale structure resulting from segregation of the polar and nonpolar components of the ionic liquids, which is enhanced by longer alkyl chains with a corresponding increase in the length scale.[37] Recently, Hayes et al. performed neutron scattering experiments with the empirical potential structure refinement (EPSR) analysis for a series of selectively deuterated $[C_2Am^+][NO_3^-]$ and its analogue with a terminal hydroxyl group ethanolammonium nitrate $[C_2OHAm^+][NO_3^-]$.[38] According to their EPSR analyses, $[C_2Am^+][NO_3^-]$ has well-defined local organization of the charged and uncharged moieties, and a bicontinuous "*sponge*" structure forms in the bulk.

Although a nanoscale segregated structure and/or structural heterogeneity of $[C_2Am^+][NO_3^-]$ were accepted in the field of ionic liquid chemistry, the origin of the specific low Q peak observed for this class of PILs remains unclear. Currently, a similar situation has been recognized in terms of assignment or interpretation of the low Q peak of APILs with relatively longer alkyl chains. Structural heterogeneity of APILs has been revealed by MD simulations by Urahata,[39] Wang and Voth,[40−42] Lopes and Padua,[43,44] and Bhargava et al.[45] Triolo et al.[46−51] have found the low Q peak appeared in the SAXS profile for a variety of APILs with an intermediate long alkyl chain, which is similar to the results for the imidazolium based ionic liquids with a longer alkyl chain. They proposed micelle-like domain formation due to the alkyl group aggregation in APILs based on the correlation length dependence on the alkyl chain length. Recent neutron diffraction experiments with the EPSR analysis done by Hardacre et al.[52] and large scale MD simulations by Margulis and co-workers[53] suggest that the low Q peak is hardly explained in terms of the formation of micelle-like aggregates; i.e., the low Q peak reflects the characteristic distance between the charged groups separated by the long alkyl chains. Collaborated works by the Castner and Margulis groups also supported recent assignment or interpretation of the low Q peaks.[54−56] Aoun et al. reasonably reproduced the low Q peak with MD simulations, which are actually observed with the high-energy X-ray diffraction (HEXRD) experiments.[57,58] We note that the heterogeneous liquid structure in PILs may play an important role in ion transport property, particularly in proton transfer and solvation in this class of ionic liquids. Therefore, it may be more crucial to elucidate the origin of the low Q peak of PILs.

In this paper, to yield further insight into the nanoscale segregation of PILs, liquid structure, and the closest ion−ion interactions, a series of PILs $[C_nAm^+][NO_3^-]$ with varying alkyl chain lengths n = 2, 3, and 4 (Chart 1) were studied by the HEXRD experiments and MD simulations. Here, we introduced a new data analysis of experimental X-ray data; structure factor intensity at a given Q_{peak} as a function of distance r (actually, integration range maximum r_{max}), $S^{Q_{peak}}(r_{max})$, by which we experimentally demonstrated how the low Q peaks are intensified corresponding to the liquid density fluctuation depending on the distance. In addition, short-range ion−ion interactions in $[C_nAm^+][NO_3^-]$ were also discussed with the aid of previously reported neutron data and MD simulations.

Chart 1. Schematic Illustrations of Ion Structures: (a) $[C_2Am^+]$, (b) $[C_3Am^+]$, (c) $[C_4Am^+]$, and (d) $[NO_3^-]$

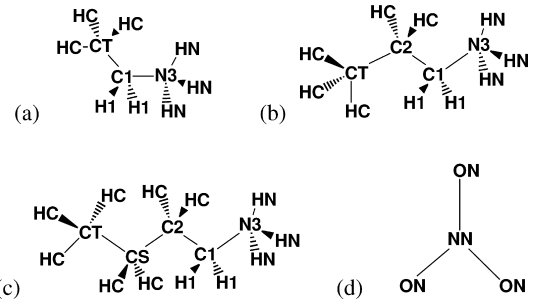

EXPERIMENTAL SECTION

Materials. Samples $[C_nAm^+][NO_3^-]$ (n = 2, 3, and 4) were prepared by the ordinary method which was described in refs 30 and 31. The water content of the sample ionic liquids was checked to be less than 100 ppm by the Karl Fischer titration method. The densities of the samples were measured by a vibration tube densimeter (Kyoto Electronics, DA-310) at 298.15 K with a temperature fluctuation of 0.01 K. The obtained density values are given in Table S2 in the Supporting Information, which are in good agreement with the literature data.[14,22,36,37,59,60]

High-Energy X-ray Diffraction Measurement and Data Analysis. The HEXRD measurements were carried out at the

dx.doi.org/10.1021/jp209561t | J. Phys. Chem. B 2012, 116, 2801−2813

high-energy X-ray diffraction beamline BL04B2 of SPring-8.[61,62] The monochromatic X-ray of 61.7 keV was obtained using a Si(220) monochromator. The observed X-ray intensity was corrected for absorption,[63] polarization, and incoherent scatterings[64] to obtain coherent scattering intensity, $I_{coh}(Q)$. The detailed procedure of data analysis is described elsewhere.[62] X-ray structure factor $S^{HEXRD}(Q)$ and X-ray radial distribution function $G(r)$ per stoichiometric volume were obtained according to

$$S^{HEXRD}(Q) = \frac{I_{coh}(Q) - \sum n_i f_i^2(Q)}{(\sum n_i f_i(Q))^2} + 1 \quad (1)$$

$$G^{HEXRD}(r) - 1 = \frac{1}{2\pi^2 r \rho_0} \int_0^{Q_{max}} Q\{S(Q) - 1\} \sin(Qr) \exp(-WQ^2)\, dQ \quad (2)$$

where n_i and $f_i(Q)$ denote the number and the atomic scattering factor of atom i, respectively,[65] ρ_0 is the number density, and W is the damping factor.

To discuss the origin of the low Q peak, we here introduce a new useful function of $S^{Q_{peak}}(r_{max})$, X-ray structure factor intensity at a given Q_{peak} as a function of r_{max}. According to the simple definition by the mutual Fourier transform between $S(Q)$ and $G(r)$, $S^{Q_{peak}}(r_{max})$ can be easily calculated by integrating experimental $r^2[G(r) - 1]$ multiplied by $\sin(Q_{peak}r)/Q_{peak}r$ up to r_{max} as follows:

$$S^{Q_{peak}}(r_{max}) = 4\pi\rho_0 \int_0^{r_{max}} r^2[G(r) - 1] \frac{\sin(Q_{peak}r)}{Q_{peak}r} dr + 1 \quad (3)$$

Since Q_{peak} is given as the value of the observed low Q peak position, thus the integration in the eq 3 becomes just a function of r, we can easily evaluate $S^{Q_{peak}}(r_{max})$ with varying the integration range maximum up to r_{max}. For convenience, the procedure for evaluating $S^{Q_{peak}}(r_{max})$ is shown in Figure S1 in the Supporting Information.

To discuss the intermolecular interactions, we subtracted the intramolecular structure factor from the total one to yield the intermolecular one on the basis of the relationship $S^{HEXRD}(Q) = S^{HEXRD}_{intra}(Q) + S^{HEXRD}_{inter}(Q)$, where $S^{HEXRD}_{intra}(Q)$ and $S^{HEXRD}_{inter}(Q)$ represent the intra- and intermolecular structure factors, respectively. $S^{HEXRD}_{intra}(Q)$ was evaluated by the following equation:

$$S^{HEXRD}_{intra}(Q) = \sum (1 + \delta_{ij}) n_{ij} f_i(Q) f_j(Q) \frac{\sin(Qr_{ij})}{Qr_{ij}} \exp(-B_{ij}Q^2) \quad (4)$$

where δ_{ij}, n_{ij}, r_{ij}, and B_{ij} denote the Kronecker delta, the number of the intramolecular atom−atom pairs, and the distance and temperature factor (mean square displacement) of the i−j atom pair, respectively. X-ray data analyses were performed by using the program KURVLR.[66]

MD Simulations. MD simulations of an *NTP* ensemble, i.e., 256 pairs of C_nAm^+ (n = 2, 3, and 4) and NO_3^- ions in a cubic cell at 298 K and 1 atm, controlled by Nose's thermostat[67,68] and Parrinello−Rahman's barostat[69,70] were carried out. Lennard-Jones (LJ) and Coulomb terms were taken into account for the intermolecular interactions, and the corresponding parameters are listed in Table S1 in the Supporting Information. The LJ parameters employed here are those previously reported,[33] and the Lorentz−Berthelot combination rules were used. Atomic point charges were evaluated with the ChelpG method[71] based on ab initio calculations at the MP2/cc-pVTZ(-f)//HF/6-31G(d) levels of theory according to the CLaP force fields[72−76] as described in our previous publication.[33] With regard to the intramolecular interactions, bond stretching, bending and torsion energies were taken into consideration and the OPLS-AA/Amber force fields for a primary ammonium ions were used.[77,78] Those for a nitrate ion were taken from ref 79. The long-range interactions were treated by Ewald's method with the typical cutoff of 11 Å. The simulation time was 2 ns with a time step of 0.2 fs. It took 1.5 ns for the system equilibration, followed by the 0.5 ns production run. All simulations were carried out using Materials Explorer 5.0 MD program package with a graphical user interface (Fujitsu) at the Computing and Communication Center, Kyushu University.

X-ray structure factor $S^{MD}(Q)$ was calculated by eq 5.

$$\begin{cases} S^{MD}(Q) = \dfrac{\sum_i \sum_j \{n_i(n_j - 1) f_i(Q) f_j(Q)/N(N-1)\}}{\{\sum_k (n_k f_k(Q)/N)\}^2} \displaystyle\int_0^{r_{limit}} 4\pi r^2 \rho_0 (g_{ij}^{MD}(r) - 1) \frac{\sin(Qr)}{Qr} dr + 1 & (i = j) \\ S^{MD}(Q) = \dfrac{\sum_i \sum_j (2 n_i n_j f_i(Q) f_j(Q)/N^2)}{\{\sum_k (n_k f_k(Q)/N)\}^2} \displaystyle\int_0^{r_{limit}} 4\pi r^2 \rho_0 (g_{ij}^{MD}(r) - 1) \frac{\sin(Qr)}{Qr} dr + 1 & (i \neq j) \end{cases} \quad (5)$$

where ρ_0 denotes the ensemble average of the number density, and the total number of atoms in the simulation box N is given by

$$N = \sum_k n_k \quad (6)$$

In eq 5, the integration should be made up to r_{limit}, which is the maximum integration range depending on the MD simulation box size. The X-ray radial distribution function $G^{MD}(r)$ was obtained from $S^{MD}(Q)$ by a Fourier transform procedure similar to that of $S^{HEXRD}(Q)$. The simulation box sizes are 33.5, 35.6, and 37.4 Å for $[C_nAm^+][NO_3^-]$ (n = 2, 3, and 4), respectively, as an ensemble average.

Density values of simulation systems of $[C_nAm^+][NO_3^-]$ (n = 2, 3, and 4) were shown in Table S2 in the Supporting Information accompanied by the relative deviations from the experiments. Adequately small relative deviations indicate that our simulations can reasonably reproduce the liquid structure

dx.doi.org/10.1021/jp209561t | J. Phys. Chem. B 2012, 116, 2801−2813

and the ion−ion interaction in $[C_nAm^+][NO_3^-]$ (n = 2, 3, and 4) protic ionic liquids.

Ab initio Calculations. To yield further insight into the hydrogen bonding, ab initio calculations were carried out for a molecular complex and an ion pair in the gas phase at the MP2/6-311G(d,p) level of theory.[80−93] Basis set superposition error (BSSE) was corrected by using a counterpoise method.[94,95] The polarizable continuum model (PCM)[96−114] was used for these species in dielectric solutions. In the PCM calculations, atomic radii including a hydrogen atom were explicitly considered by using those in the UFF force fields.[115] For the species in dielectric solutions, the BSSE correction was also estimated with single point calculations in the gas phase for those at the optimized geometry in solutions. Normal vibration analysis was performed for all of the species at the optimized geometries except scanning potential energy surfaces to confirm they have no imaginary frequencies. The Gaussian 03 program package[116] was used all for ab initio calculations.

RESULTS AND DISCUSSION

Origin of the Low Q Peak. Figure 1 shows the total structure factors $S_{total}^{HEXRD}(Q)$'s in the Q range of $Q \leq 20$ Å^{-1} for

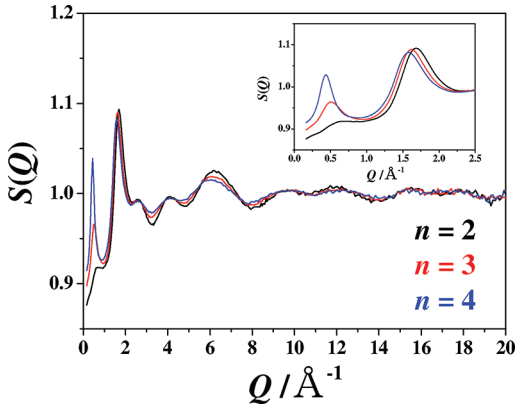

Figure 1. X-ray structure factors $S(Q)$ obtained from the HEXRD experiments of protic ionic liquids: $[C_2Am^+][NO_3^-]$ (black), $[C_3Am^+][NO_3^-]$ (red), and $[C_4Am^+][NO_3^-]$ (blue) at 298 K. Expanded $S(Q)$'s in the low Q range of Q < 2.5 Å $^{-1}$ are shown as an inserted figure.

$[C_nAm^+][NO_3^-]$ ionic liquids with n = 2−4. In the low Q range of Q < 2 Å^{-1}, all of the examined $S_{total}^{HEXRD}(Q)$'s exhibit peaks at around 0.5 and 1.6 Å^{-1}. Hereafter, we call characteristic peaks at around 0.5 Å^{-1} "the low Q peak". The low Q peaks are significantly intensified by increasing the alkyl-chain length, while the latter peaks at around 1.6 Å^{-1} are decreased in intensity. Both peaks gradually shift toward the lower Q with increasing n. On the other hand, in the higher Q range, the oscillation can be clearly observed up to 20 Å^{-1} which is obviously different from those for the other APILs in our previous studies.[33,117−121] Thus, the intramolecular structures of $[C_nAm^+][NO_3^-]$ (n = 2, 3, and 4) can be revealed by the HEXRD measurements.

The low Q peaks of about 0.5 Å^{-1} enlarged in Figure 2a, are consistent with our previous work of $[C_2Am^+][NO_3^-]$,[33] SWAXS and SANS profiles reported by Greaves et al. (for n = 2−5)[37] and small angle neutron scattering experiments by Atkin et al. (for n = 2 and 3).[36] As shown as the inset in Figure 2, the correlation length L linearly increased with the increase

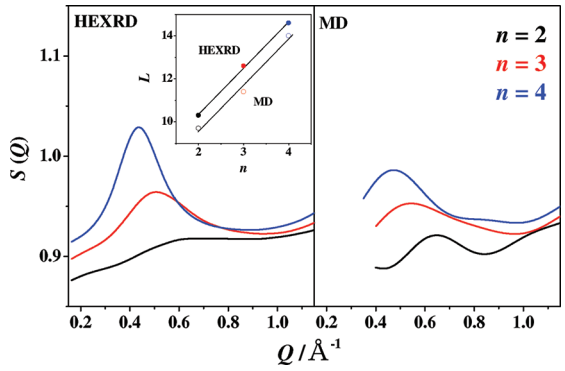

Figure 2. The low Q peaks for $[C_2Am^+][NO_3^-]$ (black), $[C_3Am^+][NO_3^-]$ (red), and $[C_4Am^+][NO_3^-]$ (blue) obtained by HEXRD experiments and by MD simulations. Correlation length L is plotted as a function of the alkyl chain length for the HEXRD experiments (closed circles) and MD simulations (open ones).

of the alkyl chain length, which is similar to that found by Greaves et al. (for n = 2−5),[37] and those for APILs by Triolo et al.[46−51] Although structural heterogeneity in ionic liquids is often discussed on the basis of such linear relationships, neutron/X-ray scattering profiles and/or structure factors for an isotropic liquid are not simple, because they are represented as the Fourier transform of overall summation of neutron/X-ray weighted real-space atom−atom correlations included in a given system, as shown by eq 5. Therefore, to discuss the low Q peak assignment, the long-range radial distribution function should be taken into account.

X-ray radial distribution functions as the form of $r^2[G(r) - 1]$ are suitable for this purpose, and those for $[C_nAm^+][NO_3^-]$ (n = 2, 3, and 4) were shown in Figure 3. Two sharp peaks in the r range of r < 3 Å can be ascribed to the intramolecular atom−atom correlations involved in the ionic liquids composing ions, as discussed in detail in our previous publication.[33] In the longer r range, two peaks appeared at about 3.4 and 4.7 Å, and three broad peaks at around 8−9, 12−

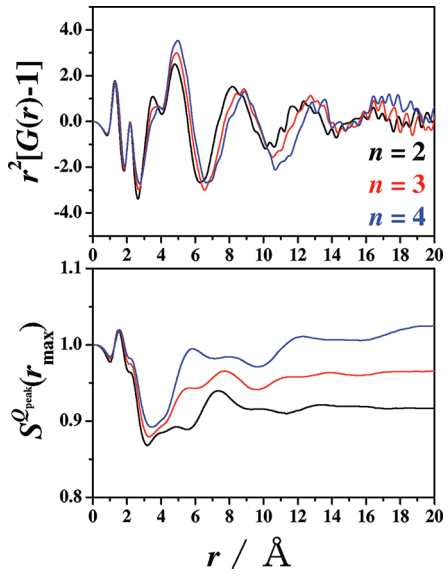

Figure 3. $r^2[G(r) - 1]$ and $S^{Q_{peak}}(r_{max})$ with Q_{peak} = 0.64 Å^{-1} for $[C_2Am^+][NO_3^-]$ (black), 0.52 Å^{-1} for $[C_3Am^+][NO_3^-]$ (red), and 0.44 Å^{-1} for $[C_4Am^+][NO_3^-]$ (blue) obtained by the HEXRD experiments.

dx.doi.org/10.1021/jp209561t | J. Phys. Chem. B 2012, 116, 2801−2813

13, and 16−18 Å apparently arose from the intermolecular atom−atom correlations. These features of $r^2[G(r) - 1]$ for $[C_2Am^+][NO_3^-]$ are in accordance with our previous study.[33] The positions of two peaks of about 3.4 and 4.7 Å were practically unchanged with varying alkyl chain length, which will be discussed in detail in the following section. On the other hand, three broad peaks in the longer r range of $r > 6$ Å noticeably shifted toward a longer side with the increase of n. We note that not only the positive peaks but also the negative valleys in $r^2[G(r) - 1]$ have a physical meaning; i.e., the spatial configurations at the peak and the valley are dense and less dense, respectively, relative to the bulk density. Thus, such spatial density oscillations can be found up to 20 Å for $[C_nAm^+][NO_3^-]$ (n = 2, 3, and 4). In addition, as shown in Figure 2, the values of L are 9.7, 11.4, and 14 Å for n = 2, 3, and 4, respectively. Nevertheless, there is no clear indication in $r^2[G(r) - 1]$ in the corresponding position to the correlation length for these ionic liquids.

For more quantitative discussion on the relationship between the low Q peak and liquid structure, it is useful to clarify the r dependence of the structure factor intensity at a given Q, i.e., $S^{Q_{peak}}(r_{max})$.[122] As shown in Figure 3, all $S^{Q_{peak}}(r_{max})$'s decreased in intensity up to about 3 Å with a peak of 1.6 Å and a shoulder of 2.1 Å, which can be clearly ascribed to the intramolecular peaks in $r^2[G(r) - 1]$. Then, the intensity of $S^{Q_{peak}}(r_{max})$ increased up to about 8−10 Å with an oscillation. The second intensity increase in $S^{Q_{peak}}(r_{max})$'s for n = 3 and 4 was found at around 10−13 Å. Furthermore, the respective $S^{Q_{peak}}(r_{max})$ intensity again increased in the r range of $r > 16$ Å except for n = 2, and finally approached the maximum height of the low Q peak. It should be noted that, at the longer r range of $r > 10$ Å, $S^{Q_{peak}}(r_{max})$ for n = 2 was practically unchanged in intensity; meanwhile, $S^{Q_{peak}}(r_{max})$'s for n = 3 and 4 were evidently intensified. Here, we also note that the r range of $10 < r/Å < 12$ corresponds to a valley in $r^2[G(r) - 1]$, not a peak, and that the valley becomes deeper with a shift toward a longer side as the increase of the alkyl chain length.

As will be described in detail in a later section, $G(r)$ can be divided into the intra- and the intermolecular parts $G_{intra}(r)$ and $G_{inter}(r)$, respectively. Similarly, as shown in Figure 4, their intra- and intermolecular contributions to $S^{Q_{peak}}(r_{max})$, $S_{intra}^{Q_{peak}}(r_{max})$ and $S_{inter}^{Q_{peak}}(r_{max})$, can be evaluated on the basis of $G_{intra}(r)$ and $G_{inter}(r)$. $S_{intra}^{Q_{peak}}(r_{max})$ values approached about 0.3−0.35 at 20 Å depending on the alkyl chain length, which evidently indicates that the intramolecular atom−atom correlations significantly contribute to the intensity of the low Q peak in $S(Q)$. On the other hand, $S_{intra}^{Q_{peak}}(r_{max})$ hardly depends on the alkyl chain length in the r range of $r < 2.5$ Å. Clearly, intensity increase of $S_{intra}^{Q_{peak}}(r_{max})$ at around 3−6 Å, where the furthest atom−atom correlations such as the ammonium and the terminal methyl groups in the C_4Am^+ cation exist, mainly contributes to the alkyl chain length dependence of $S_{intra}^{Q_{peak}}(r_{max})$ intensity. It is worth pointing out that the contribution of the intramolecular atom−atom correlations become more important when the cations have much longer alkyl chains.

$S_{inter}^{Q_{peak}}(r_{max})$ of about 0.61−0.65 in intensity at 20 Å more significantly contributes to the overall low Q peak intensity. As well as $S_{intra}^{Q_{peak}}(r_{max})$, $S_{inter}^{Q_{peak}}(r_{max})$ is practically the same in the r range of $r < 4$ Å for all of the ionic liquids examined here. In the r range of $4 < r/Å < 7$, intensity increase of $S_{inter}^{Q_{peak}}(r_{max})$ is more quick for the ionic liquid with a longer alkyl chain. Via nearly plateaus of 7−10 Å, $S_{inter}^{Q_{peak}}(r_{max})$ increased more in intensity in the r range of $r > 10$ Å with lengthening of the alkyl chain. The increase in $S_{inter}^{Q_{peak}}(r_{max})$ intensity at around 10−12 Å can be related to the valley in density oscillation at the corresponding length scale in $r^2[G(r) - 1]$, that is less dense space relative to the bulk density.

Detailed analysis has been done with the aid of MD simulations for further understanding the relationship between the low Q peak and liquid structure. X-ray structure factors for $[C_nAm^+][NO_3^-]$ (n = 2, 3, and 4) $S_{total}^{MD}(Q)$ were calculated. A comparison of simulations and experiments is shown in Figures S2−S4 in the Supporting Information in terms of the total $S_{total}^{MD}(Q)$, the intermolecular one $S_{inter}^{MD}(Q)$, and the intermolecular X-ray radial distribution function $G_{inter}^{MD}(r)$, respectively. (Please refer to the Supporting Information.) As can be seen in these figures, MD simulations reasonably agree with the experimental data except for the low Q range. The low Q peaks in $S_{total}^{MD}(Q)$ are shown in Figure 2 with the experiment for comparison. $S_{total}^{MD}(Q)$'s reproduced the observed ones at least qualitatively; i.e., peak positions of the low Q peak agree well with the experiments, as shown in the inserted figure, while deviations in the low Q peak intensity from the experiment are not negligible. Similar poor reproduction of the low Q peak in intensity has been found in the simulated structure factors for the imidazolium based APILs due to a small system size. However, as clearly shown in Figure S2 in the Supporting Information, all $S_{inter}^{MD}(Q)$'s yield shoulders of almost the same Q position with the experiment, which indicates that the simulated liquid structure involves what yields the intermolecular component contributing to the low Q peak intensity.

Figure 5b shows simulated intermolecular X-ray radial distribution functions $G_{inter}^{MD}(r)$ as the form of $r^2[G(r) - 1]$, which is accompanied by those evaluated with the experiments for comparison (Figure 5a). The long-range ordering and its alkyl chain dependence observed in these ionic liquids were well reproduced by MD simulations, though the oscillation amplitudes were slightly larger relative to the experiment. $G_{inter}^{MD}(r)$ can be divided into three terms: the cation−cation, the cation−anion, and the anion−anion $G_{inter}^{MD}(r)$'s, as shown in Figure 5c−e. As aforementioned, $S_{inter}^{Q_{peak}}(r_{max})$'s for $[C_nAm^+][NO_3^-]$ (n = 2, 3, and 4) increase in intensity at around 4−7 and 10−12 Å regions depending on the alkyl chain length.

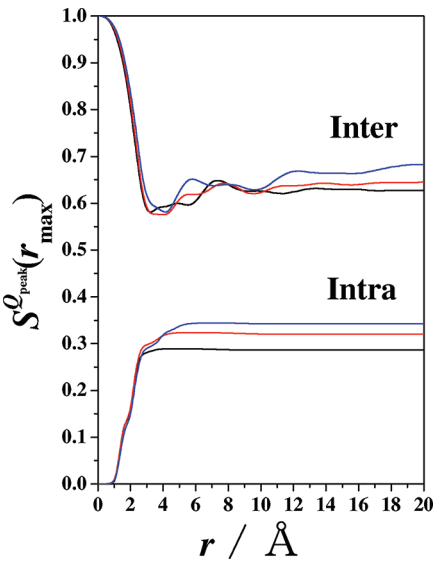

Figure 4. The inter- and intramolecular $S^{Q_{peak}}(r_{max})$ for $[C_2Am^+][NO_3^-]$ (black), $[C_3Am^+][NO_3^-]$ (red), and $[C_4Am^+][NO_3^-]$ (blue).

dx.doi.org/10.1021/jp209561t | J. Phys. Chem. B 2012, 116, 2801−2813

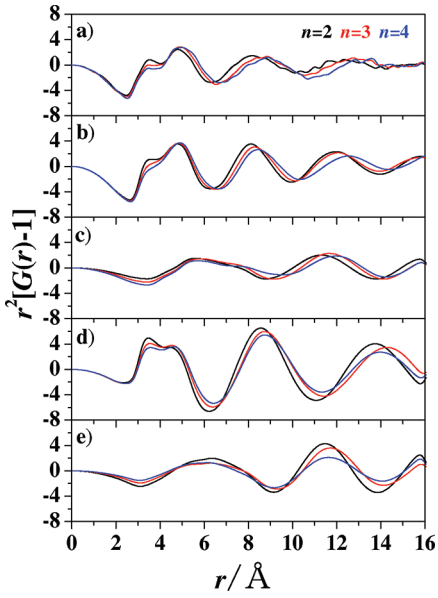

Figure 5. $r^2[G(r) - 1]$ obtained by the HEXRD experiments (a) and MD simulations (b) and those divided into the cation−cation (c), the cation−anion (d), and the anion−anion (e). $[C_2Am^+][NO_3^-]$ (black), $[C_3Am^+][NO_3^-]$ (red), and $[C_4Am^+][NO_3^-]$ (blue).

Looking at the r range of 4−7 Å, the intermolecular cation−cation $r^2[G^{MD}_{inter}(r) - 1]$ is practically unchanged and independent from the alkyl chain length. Thus, the existence of this length scale alkyl chain aggregates is unclear. Nevertheless, in the cation−anion $r^2[G^{MD}_{inter}(r) - 1]$, the intensity decreased in this r range with lengthening the alkyl chain, which looks like the first neighboring broad peak of about 4 Å (involving a peak of 3.4 Å and a shoulder of 4.7 Å) shifts toward the further side. In addition, the first broad peak at around 6 Å in the intermolecular anion−anion $r^2[G^{MD}_{inter}(r) - 1]$ decreased in intensity for a longer alkyl chain. These variations could be interpreted as follows: the first neighboring cation−anion correlations shift toward the further side to decrease the density of the intermolecular anion−anion correlations in further length scale as the increase of the alkyl chain length. This suppressed the density of the second neighboring anion−anion correlations is contributable the low Q peak intensity, as shown in Figure 5. The broad peak of the first neighboring cation−anion correlation may be related to their orientation and/or configuration, which will be discussed in detail from the atom−atom pair correlation functions in a later section.

In the 10−12 Å length scale, the second oscillation peaks were found in $r^2[G^{MD}_{inter}(r) - 1]$ for like ions and the third valley appeared in unlike ions' $r^2[G^{MD}_{inter}(r) - 1]$. The former decreased in intensity, while the latter increased with increasing n. In addition, the density decrease found in the anion−anion $r^2[G^{MD}_{inter}(r) - 1]$ was relatively larger than the other. Therefore, it is suggested that the excluded cation−cation and anion−anion correlations in this length scale yield the low Q peak enlargement with lengthening of the alkyl chain, accompanied by suppressing the oscillation amplitude of the cation−anion correlation. It also suggested that the observed low Q peaks for $[C_nAm^+][NO_3^-]$ (n = 2, 3, and 4) could be explained without assuming the formation of spherical and/or spheroidal domains like micelles whose length scale is characterized with the correlation length L. This is clearly supported with the MD

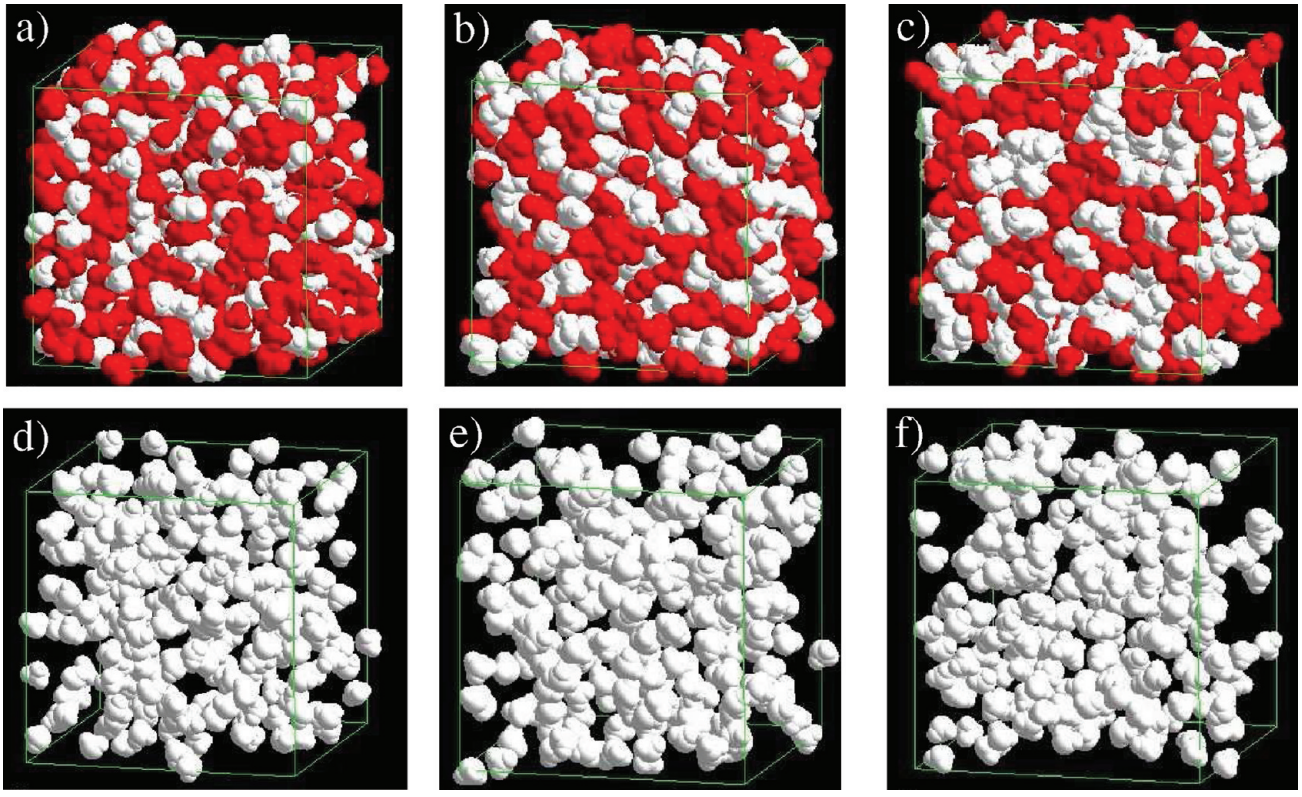

Figure 6. Typical snapshots of $[C_2Am^+][NO_3^-]$ (a), $[C_3Am^+][NO_3^-]$ (b), and $[C_4Am^+][NO_3^-]$ (c), where the ammonium groups in cations and the nitrate ions are colored by red and the respective alkyl chains are colored by white, respectively. The snapshots of $[C_2Am^+][NO_3^-]$ (d), $[C_3Am^+][NO_3^-]$ (e), and $[C_4Am^+][NO_3^-]$ (f) with only the terminal methyl groups of ammonium are represented.

dx.doi.org/10.1021/jp209561t | J. Phys. Chem. B 2012, 116, 2801−2813

snapshots shown in Figure 6, where the terminal methyl groups in the cations are solely shown as Figure 6d–f. Taking into consideration the averaged simulation box sizes of 33.5, 35.6, and 37.4 Å for n = 2, 3, and 4, respectively, much smaller channel-like aggregated alkyl chains disperse in the simulation box.

Short Range Cation–Anion Interactions. To shed light onto the short-range ion–ion interactions in the $[C_nAm^+][NO_3^-]$ (n = 2, 3, and 4), the intermolecular radial distribution function $G_{inter}(r)$ was evaluated by means of the HEXRD experiments and MD simulations, as shown in Figure 7 in the r range of 1.5 < r/Å < 10, and also the comparison between the experiment and MD is shown in Figure S4 in the Supporting Information. Experimental $G_{inter}(r)$ was obtained by similar procedures considering conformations of ions described in our previous publication.[33] Estimated intramolecular structure factors $S_{intra}(Q)$'s were shown in Figure S5 in the Supporting Information. As shown in Figure 7a, $G_{inter}(r)$'s for $[C_nAm^+][NO_3^-]$ (n = 2, 3, and 4) show a shoulder of about 3.0 Å, two broad peaks of 3.4 and 4.7 Å regardless of n, and a rather broad peak at around 8.0–8.5 Å. These features in $G_{inter}(r)$ for n = 2 agree well with previously reported $G_{inter}(r)$ obtained by a large angle X-ray experiment.[33] All peak positions are almost the same among the ionic liquids examined in this study. In addition, intensities in $G_{inter}(r)$ ranging 2.0 < r/Å < 3.0 are practically the same, which suggests that the closest atom–atom correlations in the nearest neighboring cation–anion are practically independent from the alkyl chain length. On the other hand, it should be noted that the intensity of $G_{inter}(r)$ decreased in the r ranges of 3.0 < r/Å < 4.4 and 6.5 < r/Å < 9, while they slightly increased in 4.5 < r/Å < 6.5 with lengthening of the alkyl chain. These variations suggest that small but significant variations occur in the further atom–atom correlations involved in the nearest neighboring cation–anion interactions with increasing alkyl chain length. However, it is quite difficult to analyze such tiny variations in the experimental $G_{inter}(r)$ without molecular simulations.

All of the $G_{inter}(r)$'s for $[C_nAm^+][NO_3^-]$ (n = 2, 3, and 4) from MD simulations are in good accordance with the experimental data, so we can interpret the observed $G_{inter}(r)$ values on the basis of the atom–atom pair correlation functions $g_{X-Y}(r)$ from MD simulations. Moreover, the spatial distribu-

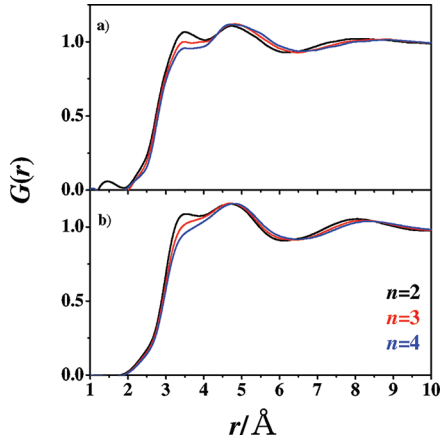

Figure 7. Intermolecular X-ray radial distribution functions extracted by the HEXRD experiments (a) and derived from the MD simulations (b). $[C_2Am^+][NO_3^-]$ (black), $[C_3Am^+][NO_3^-]$ (red), and $[C_4Am^+][NO_3^-]$ (blue).

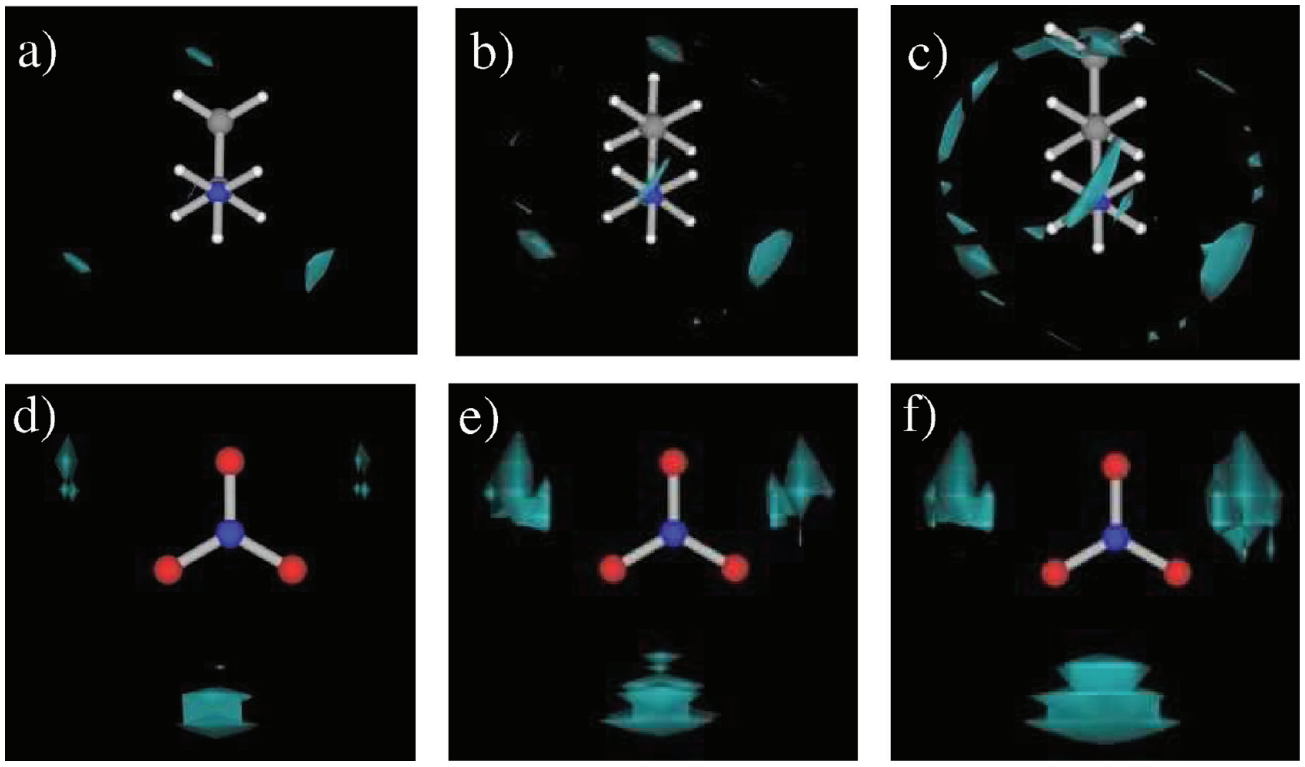

Figure 8. Spatial distribution functions of the oxygen atom in the nitrate ions around the nitrogen atom in the cations of $[C_2Am^+][NO_3^-]$ (a), $[C_3Am^+][NO_3^-]$ (b), and $[C_4Am^+][NO_3^-]$ (c), respectively, and those of the hydrogen atom in the ammonium group of the cation around the nitrogen atom in the nitrate ions of $[C_2Am^+][NO_3^-]$ (d), $[C_3Am^+][NO_3^-]$ (e), and $[C_4Am^+][NO_3^-]$ (f), respectively. Blue clouds show the probability of the oxygen atom in anions or the hydrogen atom in cations.

dx.doi.org/10.1021/jp209561t | J. Phys. Chem. B 2012, 116, 2801–2813

tion function SDF is a useful tool to catch the closest cation−anion interactions qualitatively, as shown in Figure 8. As can be obviously seen in Figure 8, the closest cation−anion correlations in $[C_nAm^+][NO_3^-]$ (n = 2, 3, and 4) can be mainly attributed to three NH···O hydrogen bonds between an ammonium group of C_nAm^+ and NO_3^-, as expected, which are independent from the alkyl chain length. Among them, one is the strongest followed by the other two of similar ones. Figure 8d−f undoubtedly indicate that the N−O−H angle is about 120° in the NH···O hydrogen bonding, which is consistent with a lone pair orientation in the sp^2 oxygen of a nitrate anion. However, Figure 8a−c clearly suggests the NH···O hydrogen bond is noticeably distorted; i.e., there is no high probability of a nitrate oxygen at the orientation facing the NH hydrogen. In other words, the N−H−O angle corresponding to the NH···O hydrogen bonding between C_nAm^+ and NO_3^- should have a value less than 180°. Similar distorted C_2H−X hydrogen bonding between dialkylimidazolium and various anions in aprotic ionic liquids has been so far reported since the pioneering works of ab initio calculations,[123] molecular simulations,[124] and neutron diffraction experiments with the EPSR analysis.[125] According to Tsuzuki et al.[126−128] and Enomoto et al.,[129] the distorted hydrogen bonding found in ionic liquids has been explained on the basis of the charge−charge electrostatic interaction of no orientation preference that predominantly contributes to the C_2H−X hydrogen bonding. Such distorted hydrogen bonding of the N−H−O angle less than 180° found in protic ionic liquids $[C_nAm^+][NO_3^-]$ (n = 2, 3, and 4) will be discussed in detail in a later section.

Representative and other $g_{X-Y}(r)$ for $[C_nAm^+][NO_3^-]$ (n = 2, 3, and 4) from MD simulations are shown in Figure 9 and

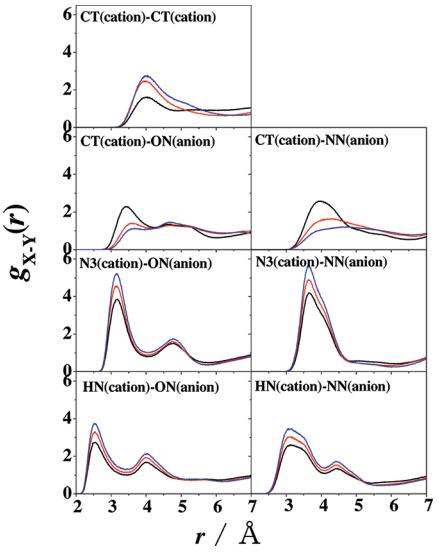

Figure 9. Typical partial atom−atom pair correlation functions $g_{X-Y}(r)$ for $[C_2Am^+][NO_3^-]$ (black), $[C_3Am^+][NO_3^-]$ (red), and $[C_4Am^+][NO_3^-]$ (blue).

Figure S8 in the Supporting Information, respectively. Peak positions and coordination numbers as an integral intensity are listed in Table 1. Interestingly, although intensities are practically the same in the r range of 2.0 < r/Å < 3.0 and decrease in 3.0 < r/Å < 4.4 in the experimental $G_{inter}(r)$, respectively, the first peaks in $g_{X-Y}(r)$ corresponding to the closest atom−atom pair correlations due to the NH···O hydrogen bonding considerably increased in intensity with no significant shift in peak position with the increase of the alkyl chain length. However, as shown in Table 1, a coordination number for the NH···O hydrogen bonding is practically regardless of the alkyl chain length though the large intensity increase in $g_{X-Y}(r)$. We note again the variations in both intensity and peak position found in $G_{inter}(r)$'s from MD simulations well agree with those observed by the HEXRD experiments. Therefore, it should be emphasized that the experimentally observed intensity decrease in $G_{inter}(r)$ of the r ranges of 3.0 < r/Å < 4.4 cannot be simply ascribed to the decreased hydrogen bonding in number for the longer alkyl chain ionic liquids.

Here, we also note that $[C_nAm^+][NO_3^-]$ (n = 2, 3, and 4) shows the low Q peak attributable to an indirect sign of the alkyl chain aggregations. The alkyl chain aggregation in these ionic liquids is clearly shown in pair correlation functions between the terminal methyl groups $g_{X-Y}(r)$ (X = Y = CT). The first peak of 3.9−4.0 Å in $g_{X-Y}(r)$ (X = Y = CT) increased in intensity by lengthening the alkyl chain. On the other hand, the first peak at r = 3.4 Å in $g_{X-Y}(r)$ (X = CT and Y = ON) can be obviously observed for $[C_2Am^+][NO_3^-]$, while no significant peak appeared in the corresponding r range for $[C_nAm^+][NO_3^-]$ (n = 3 and 4). Similarly, in $g_{X-Y}(r)$ (X = CT and Y = NN) shown in Figure S8 in the Supporting Information, the first peak at around 4.0 Å decreased with the lengthening of the alkyl chain. All of these findings suggest that the terminal methyl group in a given cation can competitively interact with both the terminal methyl group in the other cation and the oxygen atom in nitrate anions, and that nitrate ions no longer exist around the terminal methyl group when lengthening the alkyl chain. It is worth pointing out that the anions around the nonpolar group are excluded by the alkyl chain aggregation with lengthening the alkyl chains. This picture is consistent with the low Q peak appearance, which is intensified on the basis of the decreased long-range cation−cation and anion−anion correlations excluded by the alkyl chain aggregations. Finally, we conclude that an intensity decrease of experimental $G_{inter}(r)$ in the r ranges of 3.0 < r/Å < 4.4 can be ascribed to the decreased nitrate anion population around the terminal moiety of the longer alkyl chain.

The next interesting feature of the closest cation−anion interaction is the distorted NH···O hydrogen bonds, though no clear indication was observed in the HEXRD experiments. Therefore, we discuss the distorted NH···O hydrogen bonding comparing with neutron data by Hayes et al.[38] Considering the distorted NH···O hydrogen bonds, the N−H−O and H−O−N angles are useful which can be estimated from the positions of the first peak in the corresponding $g_{X-Y}(r)$ and the intramolecular NH and NO bond lengths distributions. Such structural parameters are shown in Table 2. From ref 38, the NH···O hydrogen bonding and the intermolecular N (C_2Am^+)−O (NO_3^-) distances are reported to be 2.4 and 3.0 Å, respectively. Although an actual value is unavailable, the N−H−O angle could be estimated to be 123° from neutron data, if the possible NH intramolecular atomic distance of 1.01 Å was used. Thus, the N−H−O angle is expected to be 180°, but a much smaller angle was found, indicating the hydrogen bonds are rather distorted. As listed in Table 2, the slightly longer distances were evaluated with our MD simulations for the NH···O hydrogen bonding and the intermolecular N (C_2Am^+)−O (NO_3^-). Combining these values with the first peak position in the intramolecular N−H bond length distribution yields the N−H−O angle of 121°, which is in

dx.doi.org/10.1021/jp209561t | J. Phys. Chem. B 2012, 116, 2801−2813

Table 1. Peak Position r_0 and Corresponding Coordination Numbers (c.n.) of the Selected Atom Pairs in $[C_nAm^+][NO_3^-]$ (n = 2, 3, and 4) from MD Simulations

correlation		$[C_2Am^+][NO_3^-]$		$[C_3Am^+][NO_3^-]$		$[C_4Am^+][NO_3^-]$		
ion−ion	atom pair	r_0 (Å)	c.n.	r_0 (Å)	c.n.	r_0 (Å)	c.n.	r_{max} (Å)
cation−cation	CT−CT	3.92	2.77	3.95	3.40	3.99	3.34	5.00
cation−anion	CT−ON	3.48	6.07	3.57	3.33	3.71	2.30	4.10
	CT−NN	3.95	3.83	3.98	2.24	3.99	1.36	4.70
	N3−ON	3.18	6.14	3.16	6.00	3.18	5.82	3.70
	N3−NN	3.66	2.76	3.64	2.70	3.67	2.63	4.00
	HN−ON	2.54	2.71	2.53	2.68	2.53	2.61	4.00
	HN−NN	3.12	2.52	3.13	2.44	3.13	2.36	3.00

Table 2. Selected Geometrical Parameters of $[C_2Am^+][NO_3^-]$ as the Ensemble Average by MD Simulations and at the Optimized Geometry of a $C_2Am^+\cdots NO_3^-$ Ion Pair in the Gas Phase by ab initio Calculations at the MP2/6-311G(d,p) Level

	atomic distance (Å)				bond angle		
	MD	ND[a]	ab initio[b]		MD	ND[a]	ab initio[b]
N3−HN	1.005(7)	1.010	1.040	N3−HN−ON	121(3)	123	174.2
NN−ON	1.200(6)	1.226	1.297	HN−ON−NN	111(3)		101.6
ON−HN	2.54(3)	2.4	1.463				
N3−ON	3.18(3)	3.0	2.500				
NN−HN	3.12(3)		2.142				

[a]ON−HN and N3−ON distances and the intramolecular bond length were taken from ref 38 and from OPLS-AA, respectively. [b]Values are shown for an ion pair of $C_2H_5NH_2^+\cdots ONO_2^-$ optimized in the gas phase with fixing the NH bond length to be the value optimized in a single C_2Am^+ ion in the gas phase.

good agreement with that estimated from neutron scattering. Figure 10a displays a representative configuration of the

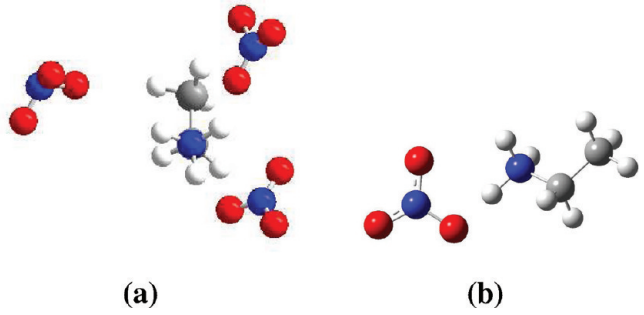

Figure 10. Representative hydrogen bonding in $[C_2Am^+][NO_3^-]$ found in MD snapshots (a) and the optimized geometry for $C_2Am^+\cdots NO_3^-$ in chloroform (ε_r = 4.9) with the PCM model (b).

ethylammonium ion surrounded by three hydrogen bonded nitrate ions found in a typical snapshot, which clearly indicates the hydrogen bonds between the cation and the anion are considerably distorted in $[C_nAm^+][NO_3^-]$ (n = 2, 3, and 4).

To discuss the nature of the distorted NH···O hydrogen bonding in $[C_nAm^+][NO_3^-]$ (n = 2, 3, and 4), ab initio calculations in the gas phase were performed at the MP2/6-311G(d,p) level of theory. As the first approach, the optimized geometries of ion paired $C_2Am^+\cdots NO_3^-$ were surveyed from various initial geometries but failed. During the geometry optimization, the NH bond in an ethylammonium cation was lengthened, followed by the proton transfer to a nitrate ion to yield a hydrogen bonded molecular complex of $C_2H_5(H_2)N\cdots HONO_2$ due to much stronger gas phase acidity of an ethylammonium ion than that of a protonated nitrate molecule.[130−135] Then, the $C_2Am^+-NO_3^-$ ion pair was optimized with a fixed N−H bond length to be the value evaluated in a single C_2Am^+ ion optimized geometry. This trial successfully worked, and obtained structural parameters are given in Table 2. Although a gas phase ion pair yields rather shorter bond lengths probably owing to overestimation by polarization, evidently linear N−H−O angle predicted in gas phase. As the second step, though rough, solvation in the ionic liquid was taken into consideration by using the PCM model with varying relative dielectric permittivity ε_r. As aforementioned, only the optimized $C_2H_5(H_2)N\cdots HONO_2$ complex was obtained in the gas phase. On the other hand, when ε_r = 4.9 (chloroform) was used, geometries for both a $C_2Am^+\cdots NO_3^-$ ion pair and a $C_2H_5(H_2)N\cdots HONO_2$ complex were successfully optimized. In acetonitrile (ε_r = 36.64), the geometry optimization for a $C_2Am^+\cdots NO_3^-$ ion pair solely succeeded. Evaluated structural parameters and binding energies are listed in Table 3, and the optimized geometry of a $C_2Am^+\cdots NO_3^-$ ion pair in chloroform is shown in Figure 10b, whose hydrogen bonding is close to linear. Thus, ab initio calculations suggest that the hydrogen bonding between C_2Am^+ and NO_3^- ions prefers a linear orientation regardless of dielectric solvation. In addition, both molecular complexes of $C_2H_5(H_2)N\cdots HONO_2$ in the gas phase and in chloroform have also practically linear N···HO hydrogen bonding, as expected.

Finally, we evaluated potential energy surfaces PESs with respect to the N−H−O angle for $C_2Am^+\cdots NO_3^-$ ion pairs in chloroform and in acetonitrile and for $C_2H_5(H_2)N\cdots HONO_2$ molecular complexes in the gas phase and in chloroform, as shown in Figure S9 in the Supporting Information. Global minima of around 180° for all PESs suggest that these hydrogen bonds prefer a linear configuration regardless of those involved whether in an ion pair or in a molecular complex. Moreover, though the potential well width for $C_2Am^+\cdots NO_3^-$ ion pairs depends on the dielectric permittivity, they are similar to those for a $C_2H_5(H_2)N\cdots HONO_2$ complex. Therefore, the NH··O hydrogen bonding in a $C_2Am^+\cdots NO_3^-$ ion pair also prefers a linear orientation in dielectric solutions, like the N···HO one in a $C_2H_5(H_2)N\cdots HONO_2$ complex. It should be

dx.doi.org/10.1021/jp209561t | J. Phys. Chem. B 2012, 116, 2801−2813

Table 3. Structural Parameters, Binding Energy E_b, and the BSSE Correction at the Optimized Geometries for a Molecular Complex of $C_2H_5NH_2\cdots HONO_2$ and an Ion Pair of $C_2H_5NH_3^+\cdots ONO_2^-$ in the Gas Phase and Dielectric Solutions at the MP2/6-311G(d,p) Level

	gas phase (ε_r = 1)	chloroform (ε_r = 4.9)		acetonitrile (ε_r = 36.64)
	molecular complex	molecular complex	ion pair	ion pair
		atomic distance (Å)		
N3−HN	1.63	1.49	1.10	1.06
NN−ON	1.36	1.34	1.29	1.28
ON−HN	1.02	1.07	1.48	1.61
N3−ON	2.65	2.56	2.58	2.66
NN−HN	1.91	1.94	2.20	2.30
		bond angle		
N3−HN−ON	175.1	174.8	177.8	170.6
HN−ON−NN	105.3	106.7	105.2	105.4
		energy		
E_b (kJ mol^{-1})	−49.6	−45.1	−108.2	−32.9
BSSE (kJ mol^{-1})	24.4	23.9	31.5	33.2

noted that the $C_2H\cdots X$ hydrogen bonds between the closest cation and anion in the dialkylimidazolium based ionic liquids have a nonlinear angle both in ion pairs in the gas phase and in ionic liquids of a liquid state. In a primary alkylammonium based ionic liquid, the NH···O hydrogen bond is significantly distorted, though those in an ion pair both in the gas phase and dielectric continuum solutions essentially prefer a linear orientation. This discrepancy should be attributed to networked hydrogen bonding structure in this kind of ionic liquids. Each primary alkylammonium cation and nitrate anion has three hydrogen donor and acceptor sites: the NH hydrogen and the oxygen, respectively. Almost all these donors and acceptors can be networked with hydrogen bonds. Such networked hydrogen bonded liquid structure is clearly shown as SDF in Figure 8, and the corresponding coordination numbers are about 3, as listed in Table 1. All of these findings suggest that the NH···O hydrogen bond increases in number to stabilize the liquid state of the ionic liquids even though it is distorted. $[C_nAm^+][NO_3^-]$ (n = 2, 3, and 4) has a networked liquid structure with as many as possible hydrogen bonds, but the NH···O hydrogen bonds are distorted.

CONCLUSIONS

To yield further insight into structural heterogeneity and ion−ion interactions of primary ammonium nitrate ionic liquids, the HEXRD experiments and MD simulations were performed for $[C_nAm^+][NO_3^-]$ (n = 2, 3, and 4).

Characteristic peaks appeared in the low Q range in both experimental and simulated $S(Q)$'s. The low Q peak was intensified with peak position shift toward lower Q with the increase of the alkyl chain length. These behaviors were analyzed with experimentally assessed $S^{Q_{peak}}(r_{max})$ and $r^2[G(r) - 1]$, which revealed that the increased intensity and the shifted peak position of the low Q peak are partially attributed to the valley at around 10−12 Å, i.e., less dense space in long-range density fluctuation in these ionic liquids. With the aid of MD simulations, this less dense space was ascribed to the excluded correlations among ions of the same sign, particularly the anion−anion, probably due to the alkyl chain aggregation

Intensities in $G_{inter}(r)$ are practically the same in the r range of 2.0 < r/Å < 3.0 among the examined ionic liquids. On the other hand, by increasing the alkyl chain length, $G_{inter}(r)$ decreased in intensity in the r ranges of 3.0 < r/Å < 4.4 and 6.5 < r/Å < 9, while it slightly increased in the r range of 4.5 < r/Å < 6.5 without peak position shift. $G_{inter}(r)$ from MD simulations was in good agreement with that evaluated from the HEXRD experiments, so that they were interpreted on the basis of $g_{X-Y}(r)$ assessed by MD simulations. Intensity decrease in the r range of 3.0−4.4 Å can be related to the decreased population of nitrate anions around the terminal methyl group when the length of the alkyl chain increases, which is in accordance with the excluded anion−anion correlation due to the alkyl chain aggregation suggested by the low Q peak appearance. These findings suggest that the terminal methyl group in the cation can competitively interact with both the terminal methyl group in the other cation and the oxygen atom in nitrate anions, and that nitrate ions no longer exist around the terminal methyl group when lengthening the alkyl chain. Hence, the anions around the nonpolar group are excluded by the alkyl chain aggregation with lengthening the alkyl chains. This picture is consistent with the low Q peak appearance; the peak intensity increase arises from the decreased long-range cation−cation and anion−anion correlations excluded by the alkyl chain aggregations.

Although it is unclear from experimental $G_{inter}(r)$, MD simulations obviously suggest the distorted NH···O hydrogen bonding of the NH···O angle about 120° that agrees well with previously reported neutron diffraction data. Ab initio calculations both in the gas phase and in dielectric solutions using the PCM model revealed that the hydrogen bonding in a molecular complex of $C_2H_5NH_2\cdots HONO_2$ (N···HO) and an ion pair of $C_2H_5NH_3^+\cdots ONO_2^-$ (NH···O) substantially prefer a linear orientation. Hence, this class of ionic liquids could be stabilized with increasing the number of the NH···O hydrogen bonds regardless of their distortion.

As a final remark, we mention our interpretation of the relationship between the low Q peak and liquid structure of protic ionic liquids $[C_nAm^+][NO_3^-]$ (n = 2, 3, and 4) on the basis of the described results. One of the most important features of PILs is not only Coulomb force but also hydrogen bonding between the closed cation and anion, by which strong networked liquid structure is formed. Hence, the NO_3^- anion prefers the charged ammonium headgroup of the cation even though the hydrogen bonds are distorted, so that the space of a characteristic length scale of 4−7 Å (less dense valley at around 6.2 Å) becomes denser when lengthening the alkyl chain. This could be rationalized with the atomistic HSAB (hard and soft acid and base) concept;[136] the atoms of higher charge density

dx.doi.org/10.1021/jp209561t | J. Phys. Chem. B 2012, 116, 2801−2813

prefer among them, for instance, the oxygen atoms in NO_3^- and the NH protons rather than the CH protons of the uncharged moieties of the alkyl chains in this case. In fact, the atomistic HSAB concept is also found in the 1-alkyl-3-methylimidazolium based ionic liquid systems.[137] As a result, the uncharged moieties of the alkyl chains may aggregate with each other, probably with a similar length scale, though experimental evidence is unclear, to acquire exothermic stabilization with van der Waals interaction. On the other hand, the first neighboring anion−anion correlations of 4−7 Å (broad peak at about 6 Å) should be excluded by thus aggregated uncharged moieties of the alkyl chains to be less dense with a shift toward further side. These spatial density variations at the relatively short r range might propagate further space; the second or the higher order dense peaks and less dense valleys in spatial density fluctuation in terms of space availability (configuration entropy in liquids). Therefore, when the alkyl chain is lengthened, dense space consisting of the second neighboring like ions with a length scale of 10−12 Å becomes less dense with a shift toward further side to produce the low Q peak in $S(Q)$. Our interpretation is somewhat speculative. Nevertheless, it may be consistent with recent structural[137] and high-accurate thermodynamic[138] studies on the 1-alkyl-3-methylimidazolium based ionic liquid systems.

■ ASSOCIATED CONTENT

Supporting Information

Additional data from the HEXRD experiments, MD simulations, and ab initio calculations. This material is available free of charge via the Internet at http://pubs.acs.org.

■ AUTHOR INFORMATION

Corresponding Author

*E-mail: yumeb@chem.kyushu-univ.jp.

Notes

The authors declare no competing financial interest.

■ ACKNOWLEDGMENTS

This work has been financially supported by Grant-in-Aids for Scientific Research No. 20350037, 23350033, and P10750, and for Scientific Research in Priority Area (Ionic Liquids) No. 20031024 from the MEXT of Japan, and Advanced Low Carbon Technology Research and Development Program (ALCA) from Japan Science and Technology Agency (JST). The synchrotron radiation experiment was carried out with the approval of the Japan Synchrotron Radiation Research Institute (JASRI) (Proposal Nos. 2007A1248 and 2007B1377). This work was carried out within the Global COE Program of Kyushu University, "Science for Future Molecular Systems".

■ REFERENCES

(1) *Ionic Liquids IV*; Brennecke, J. F., Rogers, R. D., Seddon, K. R., Eds.; American Chemical Society: Washington, DC, 2007.

(2) *Ionic Liquids in Chemical Analysis*; Koel, M., Ed; CRC Press: New York, 2009.

(3) *Ionic Liquids in Sythesis*, 2nd ed.; Wasserscheid, P., Welton, T., Eds.; VCH-Wiley: Weinheim, Germany, 2007; Vols. *1* and *2*.

(4) *Electrochemical Aspects of Ionic Liquids*; Ohno, H., Ed.; Wiley-Interscience: Hoboken, NJ, 2005.

(5) Hirao, M.; Sugimoto, H.; Ohno, H. *J. Electrochem. Soc.* **2000**, *147*, 4168.

(6) Yoshizawa, M.; Ogihara, W.; Ohno, H. *Electrochem. Solid-State Lett.* **2001**, *4*, E25.

(7) Ohno, H.; Yoshizawa, M. *Solid State Ionics* **2002**, *154−155*, 303.

(8) Susan, M. A. B. H.; Noda, A.; Mitsushima, S.; Watanabe, M. *Chem. Commun.* **2003**, 938.

(9) Noda, A.; Susan, M. A. B. H.; Kudo, K.; Mitsushima, S.; Hayamizu, K.; Watanabe, M. *J. Phys. Chem. B* **2003**, *107*, 4024.

(10) Welton, T. *Chem. Rev.* **1999**, *99*, 2071.

(11) MacFarlane, D. R.; Pringle, J. M.; Johansson, K. M.; Forsyth, S. A.; Forsyth, M. *Chem. Commun.* **2006**, 1905.

(12) Greaves, T. L.; Drummond, C. J. *Chem. Rev.* **2008**, *108*, 206.

(13) Mihichuk, L. M.; Driver, G. W.; Johnson, K. E. *ChemPhysChem* **2011**, *12*, 1622.

(14) Walden, P. *Bull. Acad. Imp. Sci.* **1914**, 1800.

(15) Xu, W.; Angell, C. A. *Science* **2003**, *302*, 422.

(16) Evans, D. F.; Yamauchi, A.; Roman, R.; Casassa, E. Z. *J. Colloid Interface Sci.* **1982**, *88*, 89.

(17) Evans, D. F.; Yamauchi, A.; Wei, G. J.; Bloomfield, V. A. *J. Phys. Chem.* **1983**, *87*, 3537.

(18) Jaeger, D. A.; Tucker, C. E. *Tetrahedron Lett.* **1989**, *30*, 1785.

(19) Byrne, N.; Wang, L.; Belieres, J.-P.; Angell, C. A. *Chem. Commun.* **2007**, 2714.

(20) Markusson, H.; Belieres, J.-P.; Johansson, P.; Angell, C. A.; Jacobsson, P. *J. Phys. Chem. A* **2007**, *111*, 8717.

(21) Shetty, P. H.; Youngberg, P. J.; Kersten, B. R.; Poole, C. F. *J. Chromatogr.* **1987**, *411*, 61.

(22) Greaves, T. L.; Weerawardena, A.; Fong, C.; Krodkiewska, I.; Drummond, C. J. *J. Phys. Chem. B* **2006**, *110*, 22479.

(23) Belieres, J.-P.; Angell, C. A. *J. Phys. Chem. B* **2007**, *111*, 4926.

(24) Poole, S. K.; Shetty, P. H.; Poole, C. F. *Anal. Chim. Acta* **1989**, *218*, 241.

(25) Thomazeau, C.; Olivier-Bourbigou, H.; Magna, L.; Luts, S.; Gilbert, B. *J. Am. Chem. Soc.* **2003**, *125*, 5264.

(26) Robert, T.; Olivier-Bourbigou, H.; Magna, L.; Gilbert, B. *ECS Trans.* **2007**, *3*, 71.

(27) Robert, T.; Magna, L.; Olivier-Bourbigou, H.; Gilbert, B. *J. Electrochem. Soc.* **2009**, *156*, F115.

(28) Yoshizawa, M.; Xu, W.; Angell, C. A. *J. Am. Chem. Soc.* **2003**, *125*, 15411.

(29) Bautista-Martinez, J. A.; Tang, L.; Belieres, J.-P.; Zeller, R.; Angell, C. A.; Friesen, C. *J. Phys. Chem. C* **2009**, *113*, 12586.

(30) Kanzaki, R.; Uchida, K.; Hara, S.; Umebayashi, Y.; Ishiguro, S.; Nomura, S. *Chem. Lett.* **2007**, *36*, 684.

(31) Kanzaki, R.; Uchida, K.; Song, X.; Umebayashi, Y.; Ishiguro, S. *Anal. Sci.* **2008**, *24*, 1347.

(32) Kanzaki, R.; Song, X.; Umebayashi, Y.; Ishiguro, S. *Chem. Lett.* **2010**, *39*, 578.

(33) Umebayashi, Y.; Chung, W.; Mitsugi, T.; Fukuda, S.; Takeuchi, M.; Fujii, K.; Takamuku, T.; Kanzaki, R.; Ishiguro, S. *J. Comput. Chem. Jpn.* **2008**, *7*, 125.

(34) Fumino, K.; Wulf, A.; Ludwig, R. *Angew. Chem., Int. Ed.* **2009**, *48*, 3184.

(35) Fumino, K.; Wulf, A.; Ludwig, R. *Phys. Chem. Chem. Phys.* **2009**, *11*, 8790.

(36) Atkin, R.; Warr, G. *J. Phys. Chem. B* **2008**, *112*, 4164.

(37) Greaves, T. L.; Kennedy, D. F.; Mudie, S. T.; Drummond, C. J. *J. Phys. Chem. B* **2010**, *114*, 10022.

(38) Hayes, R.; Imberti, S.; Warr, G. G.; Atkin, R. *Phys. Chem. Chem. Phys.* **2011**, *13*, 3237.

(39) Urahata, S. M.; Ribeiro, M. C. C. *J. Chem. Phys.* **2004**, *120*, 1855.

(40) Wang, Y.; Voth, G. A. *J. Am. Chem. Soc.* **2005**, *127*, 12192.

(41) Wang, Y.; Voth, G. A. *J. Phys. Chem. B* **2006**, *110*, 18601.

(42) Wang, Y.; Jiang, W.; Yan, T.; Voth, G. A. *Acc. Chem. Res.* **2007**, *40*, 1193.

(43) Lopes, J. N. C.; Pádua, A. A. H. *J. Phys. Chem. B* **2006**, *110*, 3330.

(44) Lopes, J. N. C.; Gomes, M. F. C.; Pádua, A. A. H. *J. Phys. Chem. B* **2006**, *110*, 16816.

(45) Bhargava, B. L.; Devane, R.; Klein, M. L.; Balasubramanian, S. *Soft Matter* **2007**, *3*, 1395.

(46) Triolo, A.; Russina, O.; Bleif, H.-J.; Cola, E. D. *J. Phys. Chem. B* **2007**, *111*, 4641.
(47) Triolo, A.; Russina, O.; Fazio, B.; Triolo, R.; Cola, E. D. *Chem. Phys. Lett.* **2008**, *457*, 362.
(48) Russina, O.; Triolo, A.; Gontrani, L.; Caminiti, R.; Xiao, D.; Hines, L. G. Jr.; Bartsch, R. A.; Quitevis, E. L.; Plechkova, N. V.; Seddon, K. R. *J. Phys.: Condens. Matter.* **2009**, *21*, 424121.
(49) Xiao, D.; Hines, L. G. Jr; Li, S.; Bartsch, R. A.; Quitrvis, E. L.; Russina, O.; Triolo, A. *J. Phys. Chem. B* **2009**, *113*, 6426.
(50) Triolo, A.; Russina, O.; Fazio, B.; Appetecchi, G. B.; Carewska, M.; Passerini, S. *J. Chem. Phys.* **2009**, *130*, 164521.
(51) Gontrani, L.; Russina, O.; Celso, F. L.; Caminiti, R.; Annat, G.; Triolo, A. *J. Phys. Chem. B* **2009**, *113*, 9235.
(52) Hardacre, C.; Holbrey, J. D.; Mullan, C. L.; Youngs, T. G. A.; Bowron, D. T. *J. Chem. Phys.* **2010**, *133*, 074510.
(53) Annapureddy, H. V. R.; Kashyap, H. K.; Biase, P. M. D.; Margulis, C. J. *J. Phys. Chem. B* **2010**, *114*, 16838.
(54) Santos, C. S.; Annapureddy, H. V. R.; Sanjeeva Murthy, N.; Kashyap, H. K.; Castner, E. W. Jr.; Margulis, C. J. *J. Chem. Phys.* **2011**, *134*, 064501.
(55) Santos, C. S.; Sanjeeva Murthy, N.; Baker, G. A.; Castner, E. W. Jr. *J. Chem. Phys.* **2011**, *134*, 121101.
(56) Kashyap, H. K.; Santos, C. S.; Annapureddy, H. V. R.; Sanjeeva Murthy, N.; Margulis, C. J.; Castner, E. W. *Faraday Discuss.* **2011**, private communication.
(57) Aoun, B.; Goldbach, A.; Kohara, S.; Wax, J.-F.; González, M. A.; Saboungi, M.-L. *J. Phys. Chem. B* **2010**, *114*, 12623.
(58) Aoun, B.; Goldbach, A.; González, M. A.; Kohara, S.; Price, D. L.; Saboungi, M.-L. *J. Chem. Phys.* **2011**, *134*, 104509.
(59) Berthod, A.; Ruiz-Angel, M. J.; Carda-Broch, S. *J. Chromatogr., A* **2008**, *1184*, 6.
(60) Poole, C. F. *J. Chromatogr., A* **2004**, *1037*, 49.
(61) Isshiki, M.; Ohishi, Y.; Goto, S.; Takeshita, K.; Takeshita, K.; Ishikawa, T. *Nucl. Instrum. Meth. A* **2001**, *467−468*, 663.
(62) Kohara, S.; Suzuya, K.; Kashihara, Y.; Matsumoto, N.; Umesaki, N.; Sakai, I. *Nucl. Instrum. Methods Phys. Res., Sect. A* **2001**, *467−468*, 1030.
(63) Sasaki, S. KEK Report 90-16, National Laboratory for High Energy Physics, Japan, 1991.
(64) Cormer, D. T.; Mann, J. B. *J. Chem. Phys.* **1967**, *47*, 1892.
(65) Aslen, E. N.; Fox, A. G. O'Keefe, M. A. *International Tables For Crystallography Vol. C*; Kluwer: Dordrecht, The Netherlands, 1999; pp 572−574.
(66) Johanson, G.; Sandstörm, M. *Chem. Scr.* **1973**, *4*, 195.
(67) Nose, S. *Mol. Phys.* **1984**, *52*, 255.
(68) Nose, S. *J. Chem. Phys.* **1984**, *81*, 511.
(69) Parrinello, M.; Rahman, A. *J. Appl. Phys.* **1981**, *52*, 7182.
(70) Parrinello, M.; Rahman, A. *Phys. Rev. Lett.* **1980**, *45*, 1196.
(71) Chirlian, L. E.; Francl, M. M. *J. Comput. Chem.* **1987**, *8*, 894.
(72) Lopes, J. N. C.; Deschamps, J.; Pádua, A. A. H. *J. Phys. Chem. B* **2004**, *108*, 2038.
(73) Lopes, J. N. C.; Pádua, A. A. H. *J. Phys. Chem. B* **2004**, *108*, 16893.
(74) Lopes, J. N. C.; Pádua, A. A. H. *J. Phys. Chem. B* **2006**, *110*, 19586.
(75) Lopes, J. N. C.; Pádua, A. A. H.; Shimizu, K. *J. Phys. Chem. B* **2008**, *112*, 5039.
(76) Shimizu, K.; Almantariotis, D.; Gomes, M. F. C.; Pádua, A. A. H.; Lopes, J. N. C. *J. Phys. Chem. B* **2010**, *114*, 3592.
(77) Cornell, W.; Cieplak, P.; Bayly, C.; Gould, I.; Merz, K.; Ferguson, D.; Spellmeyer, D.; Fox, T.; Caldwell, J.; Kollman, P. *J. Am. Chem. Soc.* **1995**, *117*, 5179.
(78) Jorgensen, W.; Maxwell, D.; Tirado-Rivers, J. *J. Am. Chem. Soc.* **1996**, *118*, 11225.
(79) Krough-Moe, J. *Acta Crystallogr.* **1956**, *9*, 351.
(80) Head-Gordon, M.; Pople, J. A.; Frisch, M. J. *Chem. Phys. Lett.* **1988**, *153*, 503.
(81) Frisch, M. J.; Head-Gordon, M.; Pople, J. A. *Chem. Phys. Lett.* **1990**, *166*, 275.
(82) Frisch, M. J.; Head-Gordon, M.; Pople, J. A. *Chem. Phys. Lett.* **1990**, *166*, 281.
(83) Head-Gordon, M.; Head-Gordon, T. *Chem. Phys. Lett.* **1994**, *220*, 122.
(84) Saebo, S.; Almlof, J. *Chem. Phys. Lett.* **1989**, *154*, 83.
(85) Krishnan, R.; Binkley, J. S.; Seeger, R.; Pople, J. A. *J. Chem. Phys.* **1980**, *72*, 650.
(86) McLean, A. D.; Chandler, G. S. *J. Chem. Phys.* **1980**, *72*, 5639.
(87) Blaudeau, J. -P.; McGrath, M. P.; Curtiss, L. A.; Radom, L. *J. Chem. Phys.* **1997**, *107*, 5016.
(88) Wachters, A. J. H. *J. Chem. Phys.* **1970**, *52*, 1033.
(89) Hay, P. J. *J. Chem. Phys.* **1977**, *66*, 4377.
(90) Raghavachari, K.; Trucks, G. W. *J. Chem. Phys.* **1989**, *91*, 1062.
(91) Binning, R. C. Jr.; Curtiss, L. A. *J. Comput. Chem.* **1990**, *11*, 1206.
(92) Curtiss, L. A.; McGrath, M. P.; Blaudeau, J. -P.; Davis, N. E.; Binning, R. C. Jr.; Radom, L. *J. Chem. Phys.* **1995**, *103*, 6104.
(93) McGrath, M. P.; Radom, L. *J. Chem. Phys.* **1991**, *94*, 511.
(94) Simon, S.; Duran, M.; Dannenberg, J. J. *J. Chem. Phys.* **1996**, *105*, 11024.
(95) Boys, S. F.; Bernardi, F. *Mol. Phys.* **1970**, *19*, 553.
(96) Miertus, S.; Scrocco, E.; Tomasi, J. *J. Chem. Phys.* **1981**, *55*, 117.
(97) Miertus, S.; Tomasi, J. *J. Chem. Phys.* **1982**, *65*, 239.
(98) Cossi, M.; Barone, V.; Cammi, R.; Tomasi, J. *Chem. Phys. Lett.* **1996**, *255*, 327.
(99) Cances, M. T.; Mennucci, B.; Tomasi, J. *J. Chem. Phys.* **1997**, *107*, 3032.
(100) Barone, V.; Cossi, M.; Tomasi, J. *J. Chem. Phys.* **1997**, *107*, 3210.
(101) Cossi, M.; Barone, V.; Mennucci, B.; Tomasi, J. *Chem. Phys. Lett.* **1998**, *286*, 253.
(102) Barone, V.; Cossi, M.; Tomasi, J. *J. Comput. Chem.* **1998**, *19*, 404.
(103) Barone, V.; Cossi, M. *J. Phys. Chem. A* **1998**, *102*, 1995.
(104) Mennucci, B.; Tomasi, J. *J. Chem. Phys.* **1997**, *106*, 5151.
(105) Tomasi, J.; Mennucci, B.; Cances, E. *THEOCHEM* **1999**, *464*, 211.
(106) Cossi, M.; Barone, V.; Robb, M. A. *J. Chem. Phys.* **1999**, *111*, 5295.
(107) Cossi, M.; Barone, V. *J. Chem. Phys.* **2000**, *112*, 2427.
(108) Cossi, M.; Rega, N.; Scalmani, G.; Barone, V. *J. Chem. Phys.* **2001**, *114*, 5691.
(109) Cossi, M.; Barone, V. *J. Chem. Phys.* **2001**, *115*, 4708.
(110) Cossi, M.; Scalmani, G.; Rega, N.; Barone, V. *J. Chem. Phys.* **2002**, *117*, 43.
(111) Cossi, M.; Rega, N.; Scalmani, G.; Barone, V. *J. Comput. Chem.* **2003**, *24*, 669.
(112) Mennucci, B.; Cances, E.; Tomasi, J. *J. Phys. Chem. B* **1997**, *101*, 10506.
(113) Cammi, R.; Mennucci, B.; Tomasi, J. *J. Phys. Chem. A* **1999**, *103*, 9100.
(114) Cammi, R.; Mennucci, B.; Tomasi, J. *J. Phys. Chem. A* **2000**, *104*, 5631.
(115) Rappe, A. K.; Casewit, C. J.; Colwell, K. S.; Goddard, W. A. III; Skiff, W. M. *J. Am. Chem. Soc.* **1992**, *114*, 10024.
(116) Frisch, M. J.; Trucks, G. W.; Schlegel, H. B.; Scuseria, G. E.; Robb, M. A.; Cheeseman, J. R.; Montgomery, J. A., Jr.; Vreven, T.; Kudin, K. N.; Burant, J. C.; Millam, J. M.; Iyengar, S. S.; Tomasi, J.; Barone, V.; Mennucci, B.; Cossi, M.; Scalmani, G.; Rega, N.; Petersson, G. A.; Nakatsuji, H.; Hada, M.; Ehara, M.; Toyota, K.; Fukuda, R.; Hasegawa, J.; Ishida, M.; Nakajima, T.; Honda, Y.; Kitao, O.; Nakai, H.; Klene, M.; Li, X.; Knox, J. E.; Hratchian, H. P.; Cross, J. B.; Bakken, V.; Adamo, C.; Jaramillo, J.; Gomperts, R.; Stratmann, R. E.; Yazyev, O.; Austin, A. J.; Cammi, R.; Pomelli, C.; Ochterski, J. W.; Ayala, P. Y.; Morokuma, K.; Voth, G. A.; Salvador, P.; Dannenberg, J. J.; Zakrzewski, V. G.; Dapprich, S.; Daniels, A. D.; Strain, M. C.; Farkas, O.; Malick, D. K.; Rabuck, A. D.; Raghavachari, K.; Foresman, J. B.; Ortiz, J. V.; Cui, Q.; Baboul, A. G.; Clifford, S.; Cioslowski, J.; Stefanov, B. B.; Liu, G.; Liashenko, A.; Piskorz, P.; Komaromi, I.;

Martin, R. L.; Fox, D. J.; Keith, T.; Al-Laham, M. A.; Peng, C. Y.; Nanayakkara, A.; Challacombe, M.; Gill, P. M. W.; Johnson, B.; Chen, W.; Wong, M. W.; Gonzalez, C.; Pople, J. A. *Gaussian 03*, revision D. 01; Gaussian, Inc.: Wallingford, CT, 2004.
(117) Fujii, K.; Soejima, Y.; Kyoshoin, Y.; Fukuda, S.; Kanzaki, R.; Umebayashi, Y.; Yamaguchi, T.; Ishiguro, S.; Takamuku, T. *J. Phys. Chem. B* **2008**, *112*, 4329.
(118) Fukuda, S.; Takeuchi, M.; Fujii, K.; Kanzaki, R.; Takamuku, T.; Chida, K.; Yamamoto, H.; Umebayashi, Y.; Ishiguro, S. *J. Mol. Liq.* **2008**, *143*, 2.
(119) Fujii, K.; Seki, S.; Fukuda, S.; Takamuku, T.; Kohara, Y.; Kameda, Y.; Umebayashi, Y.; Ishiguro, S. *J. Mol. Liq.* **2008**, *143*, 64.
(120) Kanzaki, R.; Mitsugi, T.; Fukuda, S.; Fujii, K.; Takeuchi, M.; Soejima, Y.; Takamuku, T.; Yamaguchi, T.; Umebayashi, Y.; Ishiguro, S. *J. Mol. Liq.* **2009**, *147*, 77.
(121) Fujii, K.; Mitsugi, T.; Takamuku, T.; Yamaguchi, T.; Umebayashi, Y.; Ishiguro, S. *Chem. Lett.* **2009**, *38*, 340.
(122) Fujii, K.; Kanzaki, R.; Takamuku, T.; Kameda, Y.; Kohara, S.; Kanakubo, M.; Shibayama, M.; Ishiguro, S.; Umebayashi, Y. *J. Chem. Phys.* **2011**, *135*, 244502.
(123) Dymek, C. J. Jr; Grossie, D. A.; Fratini, A. V.; Adams, W. W. *J. Mol. Struct.* **1989**, *213*, 25.
(124) Hanke, C. G.; Price, S. L.; Lynden-Bell, R. M. *Mol. Phys.* **2001**, *99*, 801.
(125) Hardacre, C.; Holbrey, J. D.; McMath, S. E. J.; Bowron, D. T.; Soper, A. K. *J. Chem. Phys.* **2003**, *118*, 273.
(126) Tsuzuki, S.; Tokuda, H.; Hayamizu, K.; Watanabe, M. *J. Phys. Chem. B* **2005**, *109*, 16474.
(127) Tsuzuki, S.; Tokuda, H.; Mikami, M. *Phys. Chem. Chem. Phys.* **2007**, *9*, 4780.
(128) Tsuzuki, S.; Arai, A. A.; Nishikawa, K. *J. Phys. Chem. B* **2008**, *112*, 7739.
(129) Enomoto, T.; Nakamori, Y.; Matsumoto, K.; Hagiwara, R. *J. Phys. Chem. C* **2011**, *115*, 4324.
(130) Koppel, I. A.; Taft, R. W.; Anvia, F.; Zhu, S.-Z.; Hu, L.-Q.; Sung, K.-S.; DesMarteau, D. D.; Yagupolskii, L. M.; Yagupolskii, Y. L.; Vlasov, V. M.; Notario, R.; Maria, P.-C. *J. Am. Chem. Soc.* **1994**, *116*, 3047.
(131) Brauman, J. I.; Blair, L. K. *J. Am. Chem. Soc.* **1969**, *91*, 2126.
(132) Brauman, J. I.; Blair, L. K. *J. Am. Chem. Soc.* **1971**, *93*, 3911.
(133) Brauman, J. I.; Blair, L. K. *J. Am. Chem. Soc.* **1971**, *93*, 3914.
(134) Meot-Ner, M.; Sieck, L. W. *J. Am. Chem. Soc.* **1991**, *113*, 4448.
(135) Hunter, E. P. L; Lias, S. G. *J. Phys. Chem. Ref. Data* **1998**, *27*, 413.
(136) Umebayashi, Y.; Hamano, H.; Seki, S.; Minofar, B.; Fujii, K.; Hayamizu, K.; Tsuzuki, S.; Kameda, Y.; Kohara, S.; Watanabe, M. *J. Phys. Chem. B* **2011**, *115*, 12179.
(137) Fujii, K.; Kanzaki, R.; Takamuku, T.; Kameda, Y.; Kohara, S.; Kanakubo, M.; Shibayama, M.; Ishiguro, S.; Umebayashi, Y. *J. Chem. Phys.* **2011**, *135*, 244502.
(138) Rocha, M. A. A.; Lima, C. F. R. A. C.; Gomes, L. R.; Schröder, B.; Coutinho, J. A. P.; Marrucho, I. M.; Esperança, J. M. S. S.; Rebelo, L. P. N; Shimizu, K.; Lopes, J. N. C.; Santos, L. M. N. B. F. *J. Phys. Chem. B* **2011**, *115*, 10919.